atic error is occurring to a similar extent in our present work, the magnetic spectral function peaks at 620 and 1400 MeV shown in Fig. 3 *might* actually represent the effects of a truncated Fourier series in fitting, say, a ρ-ω peak near 750 MeV, a ϕ at 1050 MeV, and a ρ' peak[5] at 1250 MeV. (Note that it is uncertain whether the ρ' is 1^-.) In any case, the region below 1000 MeV is not inconsistent with this interpretation. The position of the zero at 1050 MeV may well be more accurate than the positions of the peak or the dip. Finally, the value of G for the annihilation process argues for a long high energy tail on the spectral function, as in Fig. 3, rather than approximating the spectral function beyond 1000 MeV by a single pole.

Possible Experimental Consequences of Triangle Singularities in Strange-Particle Production Processes*

Y. F. Chang and S. F. Tuan

Purdue University, Lafayette, Indiana

(Received 30 June 1964)

Observable consequences of anomalous threshold singularity for triangle diagrams are examined with special reference to cases where baryon resonances of narrow width participate as an internal line in the E channel. It is found that the reaction $K^- + p \rightarrow K + \pi + \Xi$, with Ξ^* (1530) included as an internal line of the graph, offers the best experimental situation for detecting an anomalous singularity effect by studying the $(K\pi)$ mass spectrum in final state.

I. INTRODUCTION

THE actuality of anomalous singularities has long been regarded by Goldberger as a critical test of present-day notions concerning the analyticity of transition amplitudes involving production reactions.[1] Indeed, in many of the dynamical approaches to strong-interaction physics, one abandons several important concepts in conventional field theory, yet, nevertheless, assumes that the singularities of the perturbation amplitude are maintained in the correct amplitude.[2] To the extent that one knows, on the strength of perturbation theory, that amplitudes for production reactions are in general characterized by the presence of various anomalous threshold singularities, both real and complex,[3-5] it is evidently of great importance to the current theoretical premise that experimental manifestations due to these singularities be found.

Landshoff and Treiman[1] first tackled this question in connection with simple triangle diagrams such as

illustrated in Fig. 1, where E is the incoming energy, m and $\sqrt{s}$ are effective masses of particles emitting from the second and third vertices. The singularities we wish to observe are not poles, but provided they are infinites rather than simple branch points, there is hope that they can give rise to observable effects when they are close to the physical region. Landau[3] and Polkinghorne and Screaton[6] have prescribed rules that only the simplest graphs produce singularities of the infinity-type. Since the simple triangle diagrams are indeed the only graphs with three external vertices that give rise to infinities, they are the logical graphs to survey in the first instance.

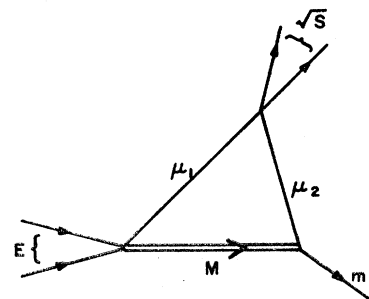The process considered by Landshoff and Treiman

FIG. 1. Basic triangle graph under consideration.

* Work supported in part by the U. S. Air Force Office of Scientific Research and the National Science Foundation.
[1] P. V. Landshoff and S. B. Treiman, Phys. Rev. 127, 649 (1962).
[2] H. P. Stapp, Phys. Rev. 125, 2139 (1962); G. Källen and A. S. Wightman, Kgl. Danske Videnskab. Selskab, Mat. Fys. Medd. 1, 6 (1958).
[3] L. D. Landau, Nucl. Phys. 13, 181 (1959).
[4] R. E. Cutkosky, J. Math. Phys. 1, 429 (1960).
[5] P. V. Landshoff and S. B. Treiman, Nuovo Cimento 19, 1249 (1961).

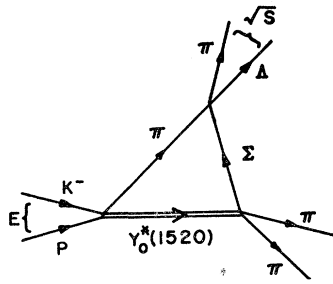[6] J. C. Polkinghorne and G. R. Screaton, Nuovo Cimento 15, 925 (1960).

FIG. 2. Triangle graph involving four-body final state $(\pi\pi\pi\Lambda)$, for incident energy $E=1660$ MeV.

involved exclusively stable particles and for practical considerations were hampered somewhat by very small cross sections, competing reactions, large distance of the singularity from the physical region, or simply rarity of the processes themselves. Variations on this approach have been proposed by Aaron[7] who introduced an unstable particle as an internal line of the graph in the s channel, thus obviating the difficulties associated with small cross sections. Halpern and Watson[8] extended this to include an unstable particle in the E channel, the crossed channel with respect to s as well. The hope here is that by considering a four-particle final state (two external particles at each vertex of the closed-loop diagram), e.g., Fig. 2, we can hope to remedy the difficulty associated with "large distance" of the singularity from the physical region as well. Aitchison[9] has questioned whether for the case of an unstable particle in the s channel, a simple application of dispersion theory or perturbation theory is completely correct. Deployment of four or more particles in the final state, despite certain advantages, must reckon with experi-
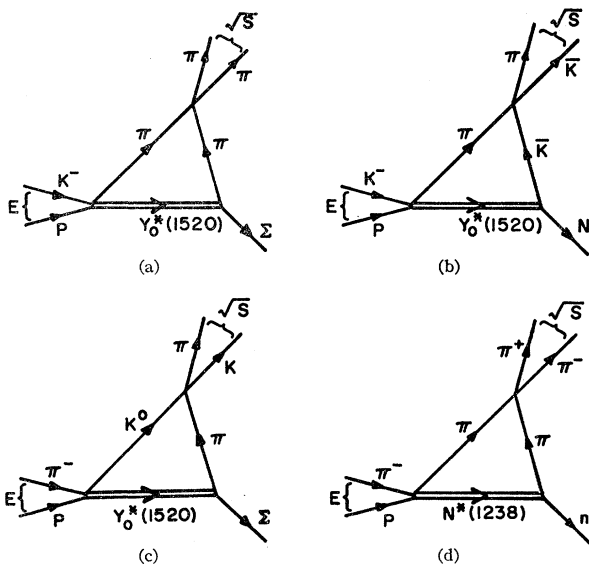

FIG. 4. Plot of square of triangle amplitude I (on arbitrary scale) against dipion mass $\sqrt{s}$ for reaction $\pi^-+p \to \pi^++\pi^-+n$ at $N^*(1238)$ production threshold $(E=1378$ MeV). The fictitious case (d') with $M=1238-5i$ is also drawn to emphasize the peaking effect due to small isobar width.

mental feasibility in terms of competing and interfering background channels open at this energy. Indeed, the detection of an anomalous singularity is likely to be quite a subtle procedure, since the effect requires usually high (and narrowly defined) incident-particle energies.

Historical interest in triangle-type graphs with an unstable particle as an internal line in the E channel actually arose from experimental impetus. Kirz, Schwartz, and Tripp[10] found that the neutron in the reaction $\pi^-p \to \pi^+\pi^-n$ comes off preferentially with a low momentum in the c.m. system; this corresponds to the $(\pi^+\pi^-)$ dipion taking up as much energy as it can—i.e., a peaking over dipion phase space at the upper end of kinematically allowed values for $\sqrt{s}$. The fact that this distortion of the phase-space spectrum was observed in the vicinity of the $\pi+N_{33}^*$ threshold (and disappeared for incidental energies far from threshold), suggests that a triangle-graph singularity of the type shown in Fig. 3(d) may be operative. Extensive calculations[9,11] have shown, however, that whereas a possible singularity candidate might exist on the physical sheet (s_a in the notation of Aitchison[9]), it cannot be near the *physical region* of s, especially at the upper end of dipion phase space, if we are to explain the experimental data; this argument is independent of the width of the (3,3) resonance. For a fictitiously small

FIG. 3. Four cases of triangle diagrams involving $Y_0^*(1520)$ and $N^*(1238)$ as an internal line in the E channel.

[7] R. Aaron, Phys. Rev. Letters **10**, 32 (1963).
[8] F. R. Halpern and H. L. Watson, Phys. Rev. **131**, 2674 (1963).
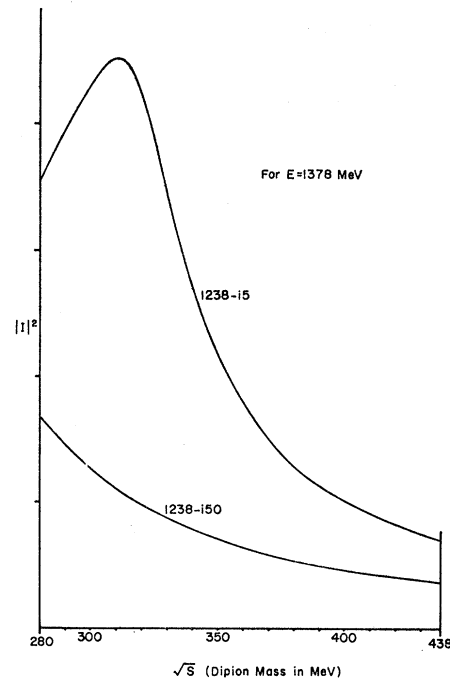[9] I. J. R. Aitchison, Phys. Rev. **133**, B1257 (1964).

[10] J. Kirz, J. Schwartz, and R. Tripp, Phys. Rev. **130**, 2481 (1963).
[11] Y. F. Chang, S. F. Tuan, and T. T. Wu (unpublished, 1963).

isobar width of N_{33}^* (say 10% of its actual width), Fig. 3(d) can give rise to an anomalous singularity (s_b in Aitchison's work[9]) which, though in the unphysical sheet below the $s=4\,\mu_\pi^2$ normal threshold branch cut of s plane, is nevertheless *near* the physical region at the low end of dipion phase space. The behavior of the squared amplitude $|I|^2$ as a function of $\sqrt{s}$ due to Fig. 3(d) is illustrated for both cases discussed above in Fig. 4; we note especially the peaking of $|I|^2$ in the neighborhood of low $\sqrt{s}$ mass values for a *narrow* isobar width; the "distance" of s_b from physical region is strongly dependent on width, as noted by Aitchison.

Fortunately, amongst the strange-particle baryon resonances recently unraveled from high-energy experiments, there are two possible candidates for the internal line M of Fig. 1 of very narrow width. The complex mass M for $\Xi_{1/2}^*(1530)$ and $Y_0^*(1520)$ assumes the following values[12]
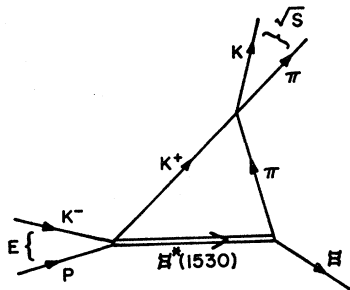
$$M(\Xi^*) = (1530-3i)\ \text{MeV},$$

$$M(Y_0^*) = (1520-8i)\ \text{MeV},$$

where $M = E_r - i\Gamma/2$. The Ξ^* case should be especially singled out for consideration, not only because of its narrow width but also because only the strong decay $\Xi^* \to \pi + \Xi$ is realized at the (M,μ_2,m) vertex (cf. Figs. 1 and 5), owing to energy conservation[13] and selection rules. The corresponding situation for $Y_0^*(1520)$ is likely to be more involved, since amongst other factors several real decay channels ($\pi\Sigma,\bar{K}N,\pi\pi\Lambda$) are open to this state with the inherent possibility for mutual interference. Other favorable features in connection with Fig. 5 will be emphasized in the body of the present paper.

The theoretical basis for the s_b-type anomalous singularity, with incident energy $E\sim\mu_1+E_r$ has been discussed by several authors[8,9]; what comes into play is a second-type singularity[14] (of the inverse-square-root type) which combines subtly with the logarithmic singularity at s_b to produce the sharp peaking effect

FIG. 6. Plot of $|I|^2$ versus $(K\pi)$ mass $\sqrt{s}$ for process $\pi^-+p \to K+\pi+\Sigma$ [Fig. 3(c)].

noticed in $|I|^2$. For convenience of reference, we have summarized briefly in Sec. II some of the results pertaining to the triangle diagram in perturbation theory. We give here some heuristic and empirical conditions that seem to determine the magnitude and position of the peak. In fact it is found upon detailed numerical analysis that under suitable conditions for values of E, m, μ_1, and μ_2 of Fig. 1, an actual *enhancement peak* for $|I|^2$ occurs in the physical interval for s with $\sqrt{s} > \mu_1 + \mu_2$, that is, not necessarily "near" the lower edge of phase space in this channel (cf. Figs. 6 and 7). That Fig. 5 falls into the new category is most gratifying, since it should improve substantially the chances of experimental detection for the phenomenon. Previous cases studied[1,8] with either stable or unstable particles in internal lines of the triangle, have tended to produce a sharp-rise type peaking at either end of the physically allowed energy range for $\sqrt{s}$, where they must *compete* with falling phase space. The dynamical

FIG. 5. An example of a triangle graph involving $K^-+p \to K+\pi+\Xi$, whose anomalous singularity is most susceptible to experimental investigation.
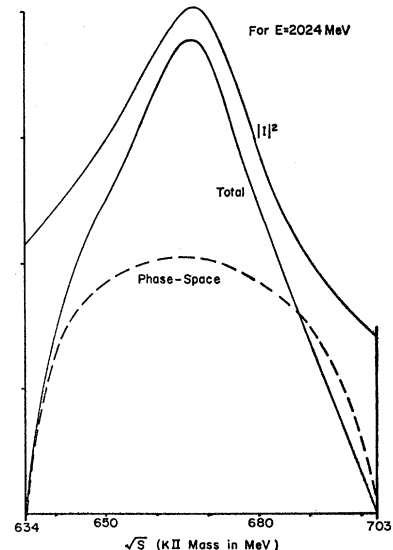
FIG. 7. Plot of $|I|^2$ and total probability of events against $(K\pi)$ mass $\sqrt{s}$ for the reaction $K^-+p \to K+\pi+\Xi$ (Fig. 5).

---

[12] For recent values of experimental width and resonances masses see, for instance, A. H. Rosenfeld, Baryon Spectroscopy, University of California Radiation Laboratory, UCRL-10897, 1963 (unpublished).

[13] There are of course possible virtual processes like $\Xi^* \to \bar{K}\Lambda$, $\bar{K}\Sigma$, but these are of scant interest in the present considerations.

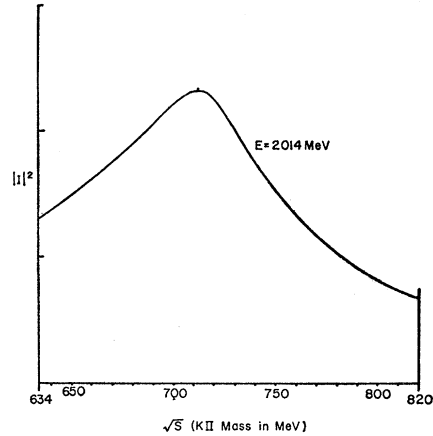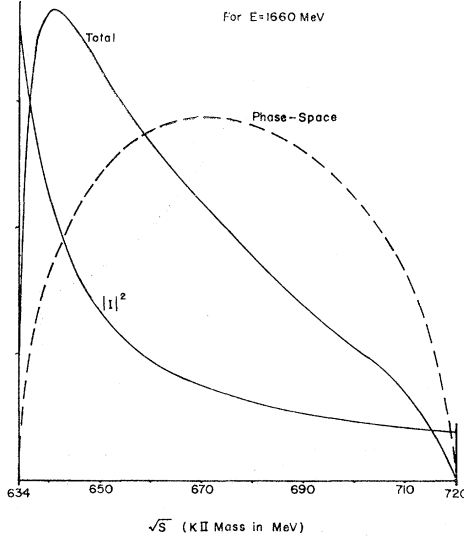[14] D. B. Fairlie, J. Nuttall, P. V. Landshoff, and J. C. Polkinghorne, J. Math. Phys. **3**, 594 (1962).

FIG. 8. Plot of $|I|^2$ and total probability of events versus $(K\pi)$ mass $\sqrt{s}$ for the reaction $K^-+p \to \bar{K}+N+\pi$ [Fig. 3(b)]. Since the scale for $|I|^2$ is arbitrary, it is the structure shape for the total probability of events that is significant.

origin and mathematical theory behind both types of peaking is of course the same in terms of complex singularity for the basic triangle diagram.

In Sec. III, the numerical results are presented for the cases shown in Figs. 5 and 3. Section IV discusses briefly the possible competing reactions and background to Fig. 5 phenomenologically. We have calculated the Feynman amplitude for the triangle graph with neglect of structure effects at the vertices, since we are concerned with the variation of the amplitude over a narrow range near the singularity. For the same reason we also neglect spin effects, treating all particles as spinless. Indeed, location of singularities from Landau rules will not be dependent upon spin, and implicit belief in these rules is the basis of the whole work. We have essentially denominator terms of form

$$1/(p_i^2+m_i^2)$$

for all internal lines, and singularities are determined therefrom. Spin effects, even for $J=\frac{3}{2}$ particles, belong to the numerator. Likewise the isospin dependence can be handled independently, with the appropriate isospin factors incorporated at each vertex in the end. With our present experimental knowledge of the relative importance of different isospin contributions to the vertices of Fig. 5, we cannot infer the preeminence of the peaking effect in one or the other of the two isospin states available to the $(K\pi)$ system.

II. TRIANGLE AMPLITUDE IN PERTURBATION THEORY

We are interested in the Feynman integral I for Fig. 1, where E is the total energy at the incident vertex, μ_1, μ_2, and M are masses for the internal lines,

a single particle m emerges from a second vertex, and the remaining particles join at a third vertex of mass $\sqrt{s}$. The energy range of interest is concentrated in the region of $E\sim\mu_1+\text{Re}(M)=\mu_1+E_r$, with $\mu_1+\mu_2\lesssim\sqrt{s} \lesssim E-m$.

The Landau singularity surface of triangle diagram (Fig. 1) is given parametrically by the equations[15]

$$E^2=M^2+\mu_1^2-2M\mu_1(u_1^2-u_2^2-u_3^2)/2u_2u_3,$$

$$m^2=M^2+\mu_2^2-2M\mu_2(u_2^2-u_1^2-u_3^2)/2u_1u_3, \quad (2.1)$$

$$\sqrt{s}=\mu_1^2+\mu_2^2-2\mu_1\mu_2(u_3^2-u_1^2-u_2^2)/2u_1u_2.$$

For the case of interest to us, the Landau singularity surface touches the physical region at point P where

$$u_2=u_1+u_3, \quad E=\mu_1+M,$$
$$m=M-\mu_2, \quad (2.2)$$
$$\sqrt{s}=\mu_1+\mu_2=\sqrt{s}_{\min}.$$

In (2.1) and (2.2), for convenience of notation, we have written M for the real part of the complex isobar mass.

The integral for the triangle diagram is

$$I=\int_0^1 d\alpha_1 \int_0^1 d\alpha_2 \int_0^1 d\alpha_3 \delta(1-\alpha_1-\alpha_2-\alpha_3)/\Delta,$$

$$\Delta=E^2\alpha_2\alpha_3+m^2\alpha_1\alpha_3+s\alpha_1\alpha_2$$
$$-(\mu_2^2\alpha_1+\mu_1^2\alpha_2+M^2\alpha_3)(\alpha_1+\alpha_2+\alpha_3). \quad (2.3)$$

We perform the α_1 integration first, then the α_2, and finally the α_3. It is evident that after doing the α_1 integration by means of the delta function, denominator Δ may be written as

$$\Delta=L[\alpha_2-(\rho+\delta_1)][\alpha_2-(\rho+\delta_2)], \quad (2.4)$$

where L, ρ, and the δ's may depend on α_3. An elementary evaluation of the α_2 integral gives

$$\frac{1}{L(\delta_1-\delta_2)} \ln\left[\frac{\alpha_2-(\rho+\delta_1)}{\alpha_2-(\rho+\delta_2)}\right]\Bigg|_0^{1-\alpha_3}. \quad (2.5)$$

The roots $\rho+\delta_1$, $\rho+\delta_2$ lie on opposite sides of the real α_2 axis and must pinch the contour to produce a physical sheet singularity. If α_2 passes the real part of these roots between the limits of the α_2 integration, 0 and $1-\alpha_3$, the phase of the logarithm will change by almost $2\pi i$ and contributes dominantly to the singularity. I is approximated by

$$I\approx 2\pi i \int \frac{d\alpha_3}{L(\delta_1-\delta_2)}, \quad (2.6)$$

where

$$L(\delta_1-\delta_2)=[A\alpha_3^2+2B\alpha_3+C]^{1/2},$$

$$A=E^4+m^4+s^2-2m^2s-2E^2m^2-2E^2s,$$

$$B=[-s^2+E^2s+m^2s+\mu_2^2s+\mu_2^2E^2 +\mu_1^2m^2+\mu_1^2s-\mu_2^2m^2-\mu_1^2E^2-2sM^2], \quad (2.7)$$

$$C=s^2+\mu_1^4+\mu_2^4-2s\mu_2^2-2s\mu_1^2-2\mu_1^2\mu_2^2.$$

---

[15] The treatment here is similar to that of Ref. 8.

At the point P, the functions A, B, C vanish identically, and in a neighborhood of P we write

$$L(\delta_1-\delta_2)=r^{1/2}f=(r_1^2+r_2^2+r_3^2)^{1/2}f, \qquad (2.8)$$

with $E-\mu_1-M=r_1e^{i\alpha}$, etc., and f a slowly varying function dependent on derivatives of $L(\delta_1-\delta_2)$ with respect to $E, m, \sqrt{s}$ at P.

It is evident that I, in a near neighborhood of P, is approximately $r^{-1/2}$ times some scale factor, and $|I|^2$ will manifest a sharp rise at the lower edge of phase space for $\sqrt{s}$ ($\approx\mu_1+\mu_2$), since $L(\delta_1-\delta_2)\equiv0$ at P. This type of behavior is exhibited by the case given in Fig. 8, as well as in some of the examples discussed by Halpern and Watson.[8]

In practice, the size and position of the peak (of which the sharply rising $|I|^2$ at $s_{\min}$ discussed above is one manifestation) in the physical range of s is determined also by internal mass conditions on μ_1 and μ_2 and the width of M, as well as on the given values of E and m. We write down here two empirical conditions[16] which must be approximately satisfied to give a peak enhancement for $|I|^2$ in the mid-range of physically allowed values of $\sqrt{s}$ (i.e., away from lower and upper edge of phase space in this channel). They are

$$\left[1+\frac{(E-m-\mu_1-\mu_2)(E+m-\mu_1-\mu_2)}{2E(\mu_1+\mu_2)}\right]^2$$
$$-1 \gtrless \frac{2}{1+(E\mu_1/uv)^{1/2}}, \qquad (2.9)$$

$$E\mu_1/uv \gtrless 9, \qquad (2.10)$$

where for simplicity we have written $M=u+iv$ $(=E_r-i\Gamma/2)$.

For purposes of numerical calculations, we write (2.3) in the following form:

$$I=\frac{1}{\sqrt{s}}\int_0^1 d\alpha_3(\tfrac{1}{2}\sqrt{Q})\ln\frac{\gamma-\sqrt{Q}}{\gamma+\sqrt{Q}}\Big|_{\gamma_a}^{\gamma_b}, \qquad (2.11)$$

where

$$-Q=-(1/4s)[(\alpha_3-1)s+\alpha_3(E^2-m^2)+\mu_2^2-\mu_1^2]^2$$
$$-\alpha_3(1-\alpha_3)E^2+\mu_1^2(1-\alpha_3)+M^2\alpha_3,$$

$$\gamma_b=[s(1-\alpha_3)+\alpha_3(E^2-m^2)+\mu_2^2-\mu_1^2]/2\sqrt{s}, \qquad (2.12)$$

$$\gamma_a=[(\alpha_3-1)s+\alpha_3(E^2-m^2)+\mu_2^2-\mu_1^2]/2\sqrt{s}.$$

For the case $\mu_1=\mu_2=\mu$, (2.12) becomes

$$-Q=-(1/4s)[(\alpha_3-1)s+\alpha_3(E^2-m^2)]^2$$
$$-\alpha_3(1-\alpha_3)E^2+\mu^2(1-\alpha_3)+M^2\alpha_3,$$

$$\gamma_b=[s(1-\alpha_3)+\alpha_3(E^2-m^2)]/2\sqrt{s}, \qquad (2.12')$$

$$\gamma_a=[(\alpha_3-1)s+\alpha_3(E^2-m^2)]/2\sqrt{s}.$$

---

[16] These conditions can be justified by elementary methods; the mathematics is, however, cumbersome, and will be discussed elsewhere.

TABLE I. The various cases described by Figs. 5 and 3 and their parameters. All energies are given in MeV.

Cases	E	m	μ_1	μ_2	M	Range of $\sqrt{s}$
(a)	1660	1194	140	140	$1520-8i$	280 to 466
(b)	1660	940	140	494	$1520-8i$	634 to 720
(c)	2014	1194	494	140	$1520-8i$	634 to 820
(d)	1378	940	140	140	$1238-50i$	280 to 438
(d')	1378	940	140	140	$1238-5i$	280 to 438
(e)	2024	1321	494	140	$1530-3i$	634 to 703

Numerical calculations of $|I|^2$ are initiated at $\alpha_3=1$, because here $\gamma_b=\gamma_a$. In the rest of the computation, we make sure the logarithm is continuous (especially its imaginary part), since our integration is over a real interval.

III. NUMERICAL RESULTS

The squares of the moduli of the amplitudes of several diagrams were evaluated over the allowable range of $\sqrt{s}$ by performing the integration given by Eq. (2.11). The calculations were performed numerically on an IBM-7090 computer using the automatic Taylor Series method developed by one of us (Y. F. Chang), which yields results of at least five-figure accuracy. Altogether, six cases are presented here to illustrate the multifarious behavior of $|I|^2$ with respect to $\sqrt{s}$. The six cases are tabulated in Table I with all their parameters: E, m, μ_1, μ_2, M, and the range of $\sqrt{s}$. Case (d') is fictitious, studied for the purpose of gaining insight into the dependence of the amplitude upon isobar width.

Figure 3(d) was the first diagram studied. The variation of $|I|^2$ with respect to $\sqrt{s}$ is shown in Fig. 4. The result is rather uninteresting so far as a peak of $|I|^2$ is concerned, no significant structure is present. Application of criteria (2.9) and (2.10) to case (d) shows (2.9) to be satisfied, but (2.10) is not satisfied. Therefore fictitious cases are studied to see how the effects due to the several parameters enter in. Case (d') differs from (d) only in that the imaginary part of M has been substantially reduced. This reduction of v yields very strong inequalities for (2.9) and (2.10). The resulting response of $|I|^2$ shows a distinct peak of 28% over its value at $\sqrt{s}_{\min}$. The conditions (2.9) and (2.10) are tabulated in Table II for all the diagrams

TABLE II. Application of conditions (2.9) and (2.10) for the various cases. The peaks are given in percent over the $|I|^2$ value at $\sqrt{s}_{\min}$. The term 'peak' here does not describe situations where $|I|^2$ shows a sharp rise for $s=s_{\min}$ as in case (b).

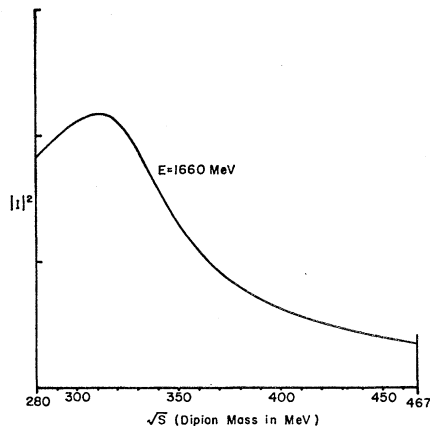| Cases	Condition (2.9)	Condition (2.10)	Remarks
(a)	$1.303>0.373$	$19.1 >9$	peak (19%)
(b)	$0.166 \not> 0.373$	$19.1 >9$	no peak
(c)	$0.411>0.199$	$81.8 >9$	peak (78%)
(d)	$1.009>0.723$	$3.116 \not> 9$	no peak
(d')	$1.009>0.304$	$31.16 >9$	peak (28%)
(e)	$0.151>0.127$	$218>9$	peak (88%)

FIG. 9. Plot of $|I|^2$, against dipion mass $\sqrt{s}$ for process $K^- + p \rightarrow \pi + \pi + \Sigma$ [Fig. 3(a)].

studied, together with the magnitude of the peaks if any. As can be easily seen, in comparing case (d) with (d'), the inequalities have been greatly strengthened by the reduction of v.

From the above analysis, one can infer that v should be as small as possible. There are two realistic baryon resonance candidates that promise to be very interesting: $Y_0^*(1520)$ and $\Xi_{1/2}^*(1530)$. We discuss first Fig. 3(b). The plot of $|I|^2$ with respect to $\sqrt{s}$ is shown in Fig. 8 together with plots of the phase space and the total probability of events. The total probability of events is the product of the phase space and $|I|^2$. In this case, criterion (2.9) is not satisfied because of the very large μ_2 mass, and the resulting $|I|^2$ does not have a peak in the sense discussed above. However, the total probability of events can have an interesting shape, due to the very sharp rise in $|I|^2$ as we approach the minimum value for $\sqrt{s}$. Diagrams similar to this case have been discussed by Landshoff and Treiman[1] and Halpern and Watson.[8]

Figure 3(a) has a μ_2 much less than that in Fig. 3(b); so in fact the left side of inequality (2.9) is substantially larger than right-hand side. Here a peak of 19% is found in $|I|^2$ with respect to its value at $\sqrt{s_{\min}}$. Figure 9 shows $|I|^2$ versus $\sqrt{s}$ for case (a). Comparison of the inequalities (Table II) for case (a) with those of case (d') shows (2.9) to be comparable, $1.009/0.304 = 3.32$ as compared with $1.303/0.373 = 3.49$, whereas the left side of (2.10) is quite different, 31.16 as compared with 19.1. Therefore (2.10) is probably more important in determining the magnitude of the peak in $|I|^2$ versus $\sqrt{s}$.

Figure 3(c) was studied to test the importance of (2.10). In this diagram, $E\mu_1$ is much larger than in Fig. 3(a). Here, condition (2.9) is relatively weak, in the sense that $0.411/0.199 = 2.07$ (cf. Table II) only, but for (2.10) the inequality ratio on the left-hand side is very large, 81.8. If comparison with cases (d') and (a) are used as a guide, the peak in $|I|^2$ against $\sqrt{s}$ should be in the neighborhood of 80%. This has indeed

been found by detailed calculations. Figure 6 shows $|I|^2$ versus $\sqrt{s}$ for case (c).

Finally, we consider case (e) (Fig. 5). This is a case where (2.10) is extremely large for the inequality ratio, 218; therefore, one would expect a tremendous peak in $|I|^2$. However (2.9) is just barely satisfied, $0.151/0.127 = 1.19$ (cf. Table II); this attenuates the peak. Figure 7 shows $|I|^2$ versus $\sqrt{s}$ for case (e). For the $K^+ + \Xi^*$ threshold value of E (2024 MeV), the peak in $|I|^2$ is 88% above its value at $\sqrt{s_{\min}}$. Apparently condition (2.9) is important when it becomes near its critical value.

Case (e) was studied in some detail because of its very attractive experimental possibilities. Figure 7 also shows plots of phase space and the total probability of events. Comparison with Fig. 8 shows a distinctly different probability of events. Figure 10 shows the behavior of $|I|^2$ versus $\sqrt{s}$ as E is varied from its threshold value. At $E = 2004$ MeV, the peak has almost completely disappeared, and the entire curve is much lower. At $E = 2044$ MeV, the peak is much larger than before. It was therefore of interest to study the behavior of the peak over the entire range of E. Figure 11 shows the locus of the peak as a function of E as it is both increased and decreased from its threshold value. This plot shows that there is an optimum value of E about 10 MeV above the threshold. The position of the peak relative to $\sqrt{s}$ is of importance, because those peaks that are very close to the minimum value of $\sqrt{s}$ will be hardly distinguishable from such responses as
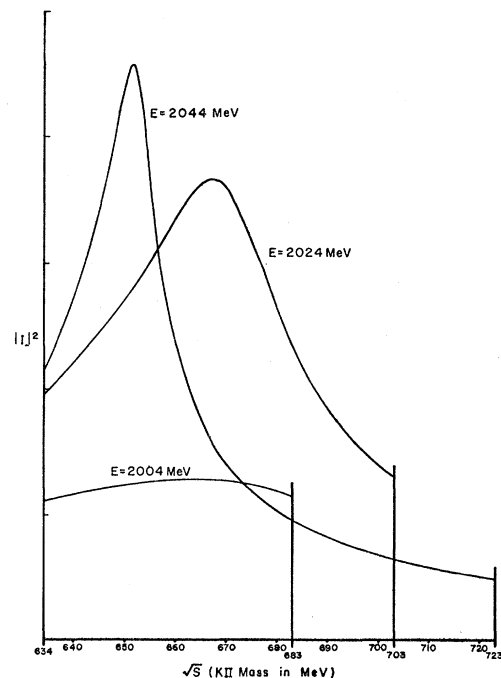

FIG. 10. The behavior of $|I|^2$ versus $\sqrt{s}$ as incident energy E is varied from its threshold value $E = 2024$ MeV for the triangle diagram (Fig. 5).
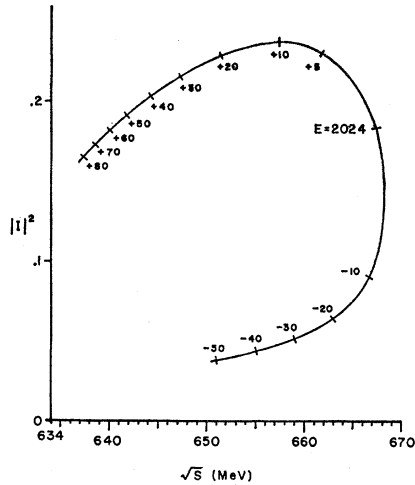
FIG. 11. The locus of peaks as a function of incident energy E for reaction $K^- + p \rightarrow K + \pi + \Xi$ via triangle graph (Fig. 5).

represented by that of Fig. 3(b), where they compete with rapidly falling phase space for experimental detection. From this point of view, the optimum value of E with respect to the position of the peak is very nearly the threshold value itself. Thus, all in all, the peak in $|I|^2$ versus $\sqrt{s}$ should be best observable for a range of E from threshold value of 2024 MeV to about 2050 MeV.

IV. DISCUSSIONS

In the last section we have detailed the numerical results. We see that the triangle diagrams due to Figs. 3(a) and 3(b), together with a diagram (cf. Fig. 2) discussed earlier,[8] can lead to very interesting structural effects for $|I|^2$ (Figs. 8 and 9). The fact that these diagrams contribute to the isospin $T=1$ state of the initial $K^- \text{-} p$ system in an important way at precisely the energy E where the resonant state $Y_1^*(1660)$ was recently found,[17] raises the question of possible interference effects between the triangle amplitudes and that of the resonant amplitude when we come to determine the quantum numbers of the latter.[18] If at threshold the $\pi + Y_0^*$ systems interact dominantly in the S state, their influence on the initial $K^- \text{-} p$ system is likely to be felt principally in $P_{3/2}$, since $Y_0^*(1520)$ has spin-parity $(\tfrac{3}{2}-)$.

Figure 3(c) and Fig. 6 represent a possible candidate for experimental investigation of a triangle singularity effect with incident $\pi^- \text{-} p$ total energy E around 2014 MeV. Table II suggests a substantial peaking for $|I|^2$, though this case must reckon with the several decay channels available to Y_0^* as discussed in the introduction.

The most promising candidate for experimental investigation is probably the triangle singularity associated with Fig. 5 and Figs. 7 and 10. As discussed in the previous sections, we are favored with a very narrow width for the Ξ^* resonance and a single, energetically allowed, strong decay channel to $\pi + \Xi$ at the second vertex, as well as suitable mass conditions on internal lines μ_1 and μ_2. Table II suggests that at $K^+ + \Xi^*$ threshold (2024 MeV), the peak is quite prominent for $|I|^2$ (88%). Also it occurs close to the center of physically allowable range for $\sqrt{s}$, which should make it particularly amenable to experiment, since one is less fettered by the problem of falling phase space competing as would be the case at $s_{\min}$ or $s_{\max}$. In fact the locus of peaks (Fig. 11) indicates that even for maximal enhancement ($E=2034$ MeV, peak $\gtrsim 100\%$), the peak position sits at around 658 MeV, as opposed to 634 for $\sqrt{s_{\min}}$.

The question of the "strength" of the triangle amplitude I, though naturally of interest from the experimental viewpoint, is much less easy to assess. For purposes of theoretical discussion, we tend to argue singularity rather than order of magnitude. However the current information[19] on Ξ^* production near threshold suggests that $K^- + p \rightarrow \Xi^* + \pi^0 + K^+$ has alone a production cross section of the order 80 μb, which compares favorably with $\pi^- + p \rightarrow \pi + N^*(1238)$ at threshold, though the latter is already the dominant channel for $(\pi^- p)$.[20] Thus we anticipate that the $(K^- p K^+ \Xi^*)$ vertex is "strong." At the second vertex, the $(\Xi^* \Xi \pi)$ coupling can be estimated from the cascade width

$$g_{\Xi^*}^2/4\pi = \tfrac{3}{2}\Gamma (E_r^2/P_\Xi^3),$$

where p_Ξ is the momentum of Ξ^* decay products in its c.m. system. There is little information on the $(K\pi K\pi)$ vertex, since we are below the energy of the K^* resonance; theoretical estimates[21] for S-wave $(K\pi)$ scattering generally yields a coupling $g_{K\pi}^2/4\pi$ of the order unity.

A little thought will show that there is no meson or vector-meson exchange between K^- and proton to give a final-state system $(K\pi\Xi)$, because of the strangeness selection rule. Thus it is expected that the most im-
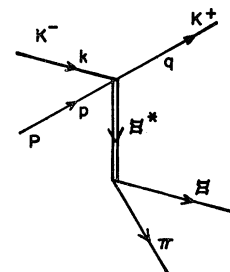

FIG. 12. Isobar diagram competing with triangle diagram of Fig. 5. Here k, p, q are the four-momenta of incident K^- and proton and final K^+, respectively.

[17] L. W. Alvarez, M. H. Alston, M. Ferro-Luzzi, D. O. Huwe, G. R. Kalbfleisch et al., Phys. Rev. Letters 10, 184 (1963).
[18] M. Taher-Zadeh, D. J. Prowse, P. E. Schlein, W. E. Slater, D. H. Stork et al., Phys. Rev. Letters 11, 470 (1963).

[19] We have benefited from a helpful discussion with Professor J. Leitner.
[20] M. Olsson and G. B. Yodh (to be published).
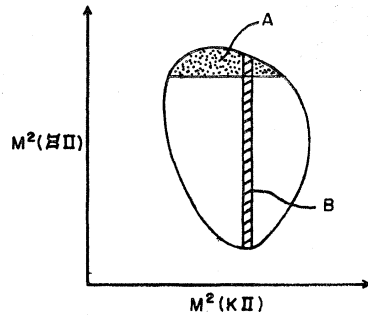[21] B. W. Lee, Phys. Rev. 120, 325 (1960).

Fig. 13. Dalitz plot for the three-body final state $(K\pi\Xi)$. The (effective mass)^2 distributions for $(\Xi\pi)$ and $(K\pi)$ are projected, respectively, on the ordinate and abscissa.

portant competing diagram to the triangle amplitude will be the isobar diagram (Fig. 12), which can certainly contribute significantly at the Ξ^* threshold of interest. A very crude estimate of the relative probability of contributions for the two processes (Figs. 2 and 12) is

$$\sim (g_{K\pi}{}^2/4\pi)|I|^2 (p+k-q)^2 - M_{\Xi^*}{}^2|^2 \sim \tfrac{1}{10}.$$

An examination of the Dalitz plot (Fig. 13) should enable us to differentiate between the two reactions. In the standard isobar picture, the $(\Xi\pi)$ has maximum mass and the K^+-meson minimum mass, and events of this type are likely to cluster around region A of Fig. 13; those due to the triangle singularity will likely distribute over region B. We are fortunate here, in that only one strong final-state interaction is present amongst the final particles $(K\pi\Xi)$: that of $(\Xi\pi)$ to form Ξ^*. This is to be contrasted with the overlapping resonance case at the $N^*(1238)$ threshold for $\pi^-+p \to \pi_1+\pi_2+N$, where $N+\pi_1$ can be important at the same time $N+\pi_2$ is important, and thus might artificially create a "resonance" in the $(\pi_1\pi_2)$ system to confound the Dalitz-plot interpretation.

Since we seek to find an anomalous singularity effect which is expected to be dominant over only a small energy range E for the initial K^--p system ($E=2024$ to 2050 MeV), a high and narrowly defined incident K^- beam is required. The momentum spread in K^- beam at this energy is about 1% (20 MeV/c) for current experiments; thus our proposal should be amenable to bubble-chamber investigation in the near future.[19] It is important to emphasize that amplitude I is inde-

pendent of the angle of emission of the Ξ particle in final state. This could be tested if one had reason to suspect that the graph in question were not in fact dominating the reaction.

In conclusion, we would like to emphasize that the basic premise of the present study is in essence implicit faith in the correctness of the Landau-Cutkosky rules and the importance of the triangle graph over other graphs of higher orders. The recent work of Bronzan,[22] which sums a particular class of scattering diagrams in the Khuri-Treiman dispersion representation[23] of a decay amplitude, is particularly to be noted in that it serves well as an example of the type of theoretical problems which are yet to be faced.

Note added in proof. It has been pointed out to us by I. J. R. Aitchison (private communication) that for an experimental effect involving the triangle singularity, we must be (a) far away from any resonance in the two-body channel looked at and (b) the triangle effect Δ must be such that compared with background it is at least 10% of unity. Both these conditions are in fact satisfied for the practical cases we propose since for Figs. 5 and 3(c), the $K^*(888)$ is far away from the $\sqrt{s}$ range of $(K\pi)$ energies we consider; in addition $\Delta_{max} = 0.16+0.2i$ and $0.20+0.07i$ for the two cases, respectively. Thus, fortuitously, the theoretical difficulties raised by J. B. Bronzan (cf. Ref. 22), are not important for the examples we discuss in the present paper. A detailed analysis of the theoretical question is given by I. J. R. Aitchison ["Final State Interactions among Three Particles" (to be published)].

[22] J. B. Bronzan, Phys. Rev. 134, B687 (1964).
[23] N. N. Khuri and S. B. Treiman, Phys. Rev. 119, 1115 (1960).